JOURNAL OF MECHANICAL ENGINEERING AND SCIENCES
ISSN: 2289-4659 e-ISSN: 2231-8380
VOLUME 18, ISSUE 4, 2024, 10233 - 10246
DOI: https://doi.org/10.15282/jmes.18.4.2024.2.0808

UNIVERSITI MALAYSIA PAHANG AL-SULTAN ABDULLAH

RESEARCH ARTICLE

Box-Behnken design application to optimize swirl effervescent droplet mean diameter

Z. A. Ghaffar[1], S. Kasolang[1]*, Ahmad H. A. Hamid[1], M. H. Mamat[2]

[1] School of Mechanical Engineering, College of Engineering, Universiti Teknologi MARA, 40450 Shah Alam, Selangor, Malaysia
[2] School of Electrical Engineering, College of Engineering, Universiti Teknologi MARA, 40450 Shah Alam, Selangor, Malaysia
Phone: +603-55435650, Fax.: +603-55435666

ABSTRACT - Swirl effervescent atomization combines the principles of swirling and bubbling liquids to create a wider spray pattern while using less liquid than traditional methods. The diameter of the resulting droplets, a key feature in atomization performance, is influenced by various dimensionless numbers, such as the gas-to-liquid ratio and the Reynolds number. A design of experiments approach was used instead of the traditional one-factor-at-a-time testing to study these factors efficiently. A novel swirl effervescent atomizer was fabricated. Shadowgraph was used to capture droplet images, and image processing was used to analyze the droplet diameter. The increase of the liquid Reynolds number from 847 to 2540 causes the Sauter mean diameter to decrease. The increase of gas Reynolds number from 0 to 1514 caused a decrease in the Sauter mean diameter. Increasing the swirl chamber length to discharge orifice diameter ratio causes an increase in Sauter mean diameter. A mathematical model was proposed and satisfies the goodness-of-fit in regression and ANOVA. Significant impacts on the droplet mean diameter were discovered by changes in the gas and liquid Reynold numbers, but the steeper reduction of the Sauter mean diameter was observed with the change of gas Reynolds number. Meanwhile, minimal effect was found to be exerted by the swirl chamber length to discharge orifice diameter ratio. The results show that the developed mathematical model can accurately predict the correlation of the Sauter mean diameter with the aforementioned factors.

ARTICLE HISTORY
Received : 08th May 2024
Revised : 12th Oct. 2024
Accepted : 05th Dec. 2024
Published : 30th Dec. 2024

KEYWORDS
Swirl effervescent atomization
Droplet mean diameter
Design of experiment
Shadowgraph
Image processing

1. INTRODUCTION

Combining multiple atomization methods within a single device has been suggested to enhance atomization performance. Kushari and Pandey [1] proposed that this approach, known as co-atomization, could address the limitations of individual atomization techniques. Swirl effervescent atomization is a specific type of co-atomization that merges swirl and effervescent atomization processes. While swirl atomization is effective for producing wide spray angles and is essential for agriculture and food processing applications, it suffers from flow rate instability. Doubling the flow rate requires a fourfold increase in pressure [2]. Conversely, effervescent atomization produces a narrow spray pattern. By combining these methods, swirl effervescent atomization achieves a wider spray angle while reducing liquid flow rates. The swirl effervescent atomization method falls under the internal mixing twin-fluid atomization category, which offers advantages such as efficient operation at low pressures, tolerance to liquid viscosity variations, and reduced gas consumption compared to external mixing [3]. A crucial parameter in atomization is the droplet mean diameter, which typically exhibits a distribution rather than a uniform value under operating conditions [2]. Factors influencing droplet mean diameter include atomizer design, operating parameters, and liquid properties. Operating conditions, atomizer design, and fluid properties can be transformed into dimensionless numbers to simplify the analysis of liquid atomization. This mathematical approach reduces the system's complexity by minimizing the number of variables needed to describe it. Research consistently highlights the gas-to-liquid ratio (GLR) as a key determinant of droplet size in twin-fluid atomizers, including swirl-effervescent atomizers [4]. Mlkvik et al. [5] corroborated this finding while categorizing internal mixing twin-fluid atomizers. Wachter et al. [6] further emphasized the dominance of GLR overpressure and liquid viscosity in external mixing systems. GLR can be defined as in Eq. (1):

$$GLR = \frac{\dot{m}_G}{\dot{m}_L} \tag{1}$$

where $\dot{m}_G$ and $\dot{m}_L$ are gas and liquid mass flow rates, respectively.

The Reynolds number primarily governs the initial breakup of the liquid jet or film into larger droplets, known as primary atomization. This phase is dominated by internal forces within the fluid, such as turbulence and momentum, which disrupt the liquid's cohesion [7]. Given that the present research focuses on twin-fluid atomization, the Reynolds values for both liquid and gas are necessary. The definition of the liquid and gas Reynolds numbers are given in Eq. (2) and Eq. (3) as defined by Lörcher et al. [8].

*CORRESPONDING AUTHOR | S. Kasolang | ✉ salmiahk@uitm.edu.my

$$Re_L = \frac{\rho_L V_L d_o}{\mu_L} \tag{1}$$

$$Re_G = \frac{\rho_G V_G d_o}{\mu_G} \tag{2}$$

where ρ_L and ρ_G are the liquid and gas densities, respectively, V_L and V_G are the liquid and gas velocities, respectively, μ_L and μ_G are the liquid and gas viscosity and d_o is the discharge orifice diameter.

Although GLR was stated earlier as an important parameter in affecting the droplet size of an atomizer, GLR was not included in this research but replaced by the Re_G, considering the equation of both parameters includes the flow rate as the numerator. In addition, Re_G was used for this research for comparison purposes with a diagram proposed by Lörcher et al. [8], which will be discussed in different articles later. The droplet diameter can also be reported as a mean diameter. The concept of the mean diameter has been generalized, and Mugele and Evans [9] standardized its notation. Their proposed equation for the calculation of mean diameter is as in Eq. (4):

$$D_{ab} = \left[\frac{\sum N_i D_i^a}{\sum N_i D_i^b}\right]^{\frac{1}{a-b}} \tag{3}$$

where a and b may take on any values corresponding to the effect investigated, i denotes the diameter range considered, N_i is the number of droplets in diameter range i, and D_i is the middle diameter of the range i. The important mean diameters are listed in Table 1, along with their fields of application, as suggested by Mugele and Evans [9].

Table 1. Droplet mean diameters and their applications

ab	Symbol	Name of mean diameter	Application
10	D_{10}	Arithmetic	Evaporation rates
20	D_{20}	Surface	Surface area controlling
30	D_{30}	Volume	Volume controlling
21	D_{21}	Surface-area-length	Absorption
31	D_{31}	Volume-length	Evaporation, molecular diffusion
32	D_{32}	Sauter mean diameter	Mass transfer, reaction
43	D_{43}	De Brouckere or Herdan	Combustion equilibrium

The Sauter mean diameter, D_{32} was chosen in this study, considering this mean diameter is applied for mass transfer, and the equation includes the surface area. Surface area is among the vital characteristics of liquid atomization since one of the purposes of atomization is to increase the surface area of a bulk liquid. A lower D_{32} indicates a larger proportion of smaller droplets [10]. Researchers proposed mathematical correlation to showcase the relation between the resultant and affecting parameters. Some examples of correlation related to Sauter mean diameter, D_{32} are proposed by Barroso et al. [11], who correlated the D_{32} of effervescent atomization, which includes the liquid Reynolds number, and another dimensionless quantity known as the Mach number, M_a, as in Eq. (5) :

$$\frac{D_{32}}{d_a} = 0.9155 \frac{\left(\frac{P_L}{P_G}\right)}{Re_L^{0.75} Ma} \tag{4}$$

where, d_a is the air inlet diameter, P_L is the liquid injection pressure, P_G is the gas injection pressure, Re_L is the liquid Reynolds number, and Ma is the Mach number, which is defined in Eq. (6):

$$Ma = \frac{V}{c} \tag{5}$$

where V is the local flow velocity, and c is the speed of sound.

Vankeswaram et al. [12] proposed the relation of D_{32} correlation with Weber number for a swirl airblast atomizer as in Eq. (7):

$$\frac{D_{32}}{t_f} = \mathrm{p}\left[\left(\frac{We_L}{We_a}\right)\sqrt{Oh}\right]^q \tag{6}$$

where, t_f is the liquid film thickness, We_L is the liquid Weber number, We_a is the air Weber number, Oh is the Ohnesorge number, p is the proportionality constant, and q is the index term.

The literature review reveals that multiple interdependent factors influence droplet mean diameter. Traditional experimental methods, which examine one factor while maintaining others constant, are time-intensive and inefficient for comprehensive analysis. Design of Experiments (DOE), a cornerstone of quality by design principles, offers a more sophisticated approach for studying droplet mean diameter in swirl effervescent atomization. This methodology enables simultaneous evaluation of multiple factors, dramatically reducing the number of experimental runs compared to

conventional sequential testing approaches. DOE facilitates systematic optimization through objective function definition, identification of critical parameters, and analysis of factor-response relationships.

Response Surface Methodology (RSM), an advanced DOE technique, enhances process understanding and optimization capabilities [13]. RSM is particularly valuable for model refinement after identifying significant factors through screening or factorial designs, especially when response surface curvature is anticipated. Among RSM approaches, the Box-Behnken Design (BBD) stands out as an independent, rotatable, or near-rotatable quadratic design that positions treatment combinations at process space edge midpoints and center [14]. A notable advantage of BBD is its exclusion of factor combinations at simultaneous extreme levels, thereby avoiding potentially unstable experimental conditions that might yield unreliable results [15].

The droplet mean diameter was analyzed using statistical analysis. A general expression of a regression model with three levels of each variable can be written as in Eq. (8) [16]:

$$y = \alpha + \beta_1 x_1 + \beta_2 x_2 + \beta_3 x_3 + \beta_{11} x_1^2 + \beta_{22} x_2^2 + \beta_{33} x_3^2 + \beta_{12} x_1 x_2 + \beta_{23} x_2 x_2 + \beta_{31} x_3 x_1 \quad (7)$$

The parameter β_i represents the linear effect of the ith factor. The parameter β_{ii} represents the quadratic effect of the ith factor, and β_{ij} represents the cross-product effect, or interaction effect, between the ith and j th factors [17]. x_1 represents the liquid Reynolds number, x_2 represents the gas Reynolds number, and x_3 represents the swirl chamber length to orifice diameter ratio.

RSM has recently been applied for experimentation in various areas, such as the pharmaceutical spray drying process for nanosuspension [18], electrospray cooling [19], dust pollution in the roadway [20], and fuel spray injection [21]. Box-Behnken design for swirl effervescent atomization was applied on various parameters such as breakup length [22], and spray angle [23]. Still, to the authors, no similar attempt has been made to investigate the droplet mean diameter. In addition, the study of droplet mean diameter for swirl effervescent atomization is scarce, with only a few available in the literature, such as Whitlow et al. [24], Jedelsky and Jicha [25], Ochowiak [26], Liu et al. [27], and Jun et al. [28]. In this work, the Box–Behnken design was used to determine the operating ranges of different factors for achieving the optimum droplet mean diameter of a newly developed swirl effervescent atomizer and propose an empirical correlation.

2. METHODS AND MATERIALS

The following section outlines the experimental methods used in characterizing effervescent swirl atomization. Section 2.1 discusses the atomizer construction. Section 2.2 addresses the test rig fabrication. Section 2.3 covers the design of the experiment. Section 2.4 explains the data extraction and analysis. Lastly, Section 2.5 describes the uncertainty analysis.

2.1 Atomizer Construction

A novel swirl effervescent atomizer was designed and fabricated. This innovative device features a unique configuration integrating tangential inlets and swirl-generating vanes into a single component. Fluids are introduced into the atomizer through the tangential inlets, where they acquire a swirling motion as they interact with the strategically positioned swirl-generating vanes. The resulting swirling fluid mixture is then directed into a conical section before being discharged through a central discharge orifice. To adjust the atomization process, the atomizer incorporates a movable stem that controls the length of the swirling chamber. By modifying the stem position, the influence of the swirl-generating vanes on the fluid can be altered. A schematic representation of this novel atomizer is presented in Figure 1.

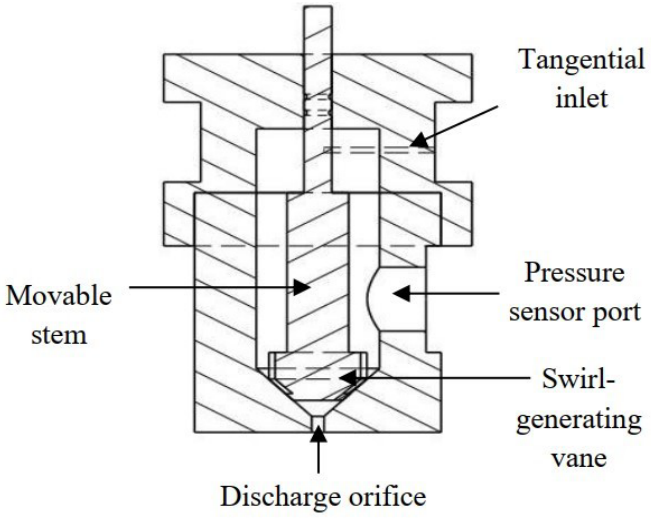

Figure 1. Schematic of the new swirl effervescent atomizer design. Adapted from [29]

2.2 Test Rig

The experimental setup utilized water as the primary fluid and compressed air as the atomizing medium. Water is sourced from a storage tank and pumped into the system by a self-priming pump. A ball valve regulates the water flow before it passes through a strainer to remove impurities. Subsequently, the water flow rate is measured by a flow sensor. An air compressor provides compressed air, and a regulator controls its pressure. The water and air lines incorporate check valves to prevent backflow and flow sensors to quantify their respective flow rates. The fluids converge at the atomizer, which is vertically oriented to direct the atomized liquid into a collection tank. The image acquisition setup consists of a high-resolution camera synchronized with a speedlight to initiate high-speed imaging of the atomization process. The image acquisition setup was also equipped with an image coordinate system. The entire experiment is overseen by a data acquisition system that collects and processes data from various sensors within the setup.

Arduino and Raspberry Pi microcontrollers were incorporated into the test rig to enhance experimental control, monitoring, and data management. Arduino, renowned for its real-time interaction with physical components, was employed to acquire sensor data and control system outputs. Arduino is an open-source electronics platform based on easy-to-use hardware and software. It allows users to read sensor inputs and control outputs like motors or LEDs, making it ideal for building interactive projects and automating tasks [30]. The Raspberry Pi, a compact yet powerful computer, was utilized for data processing and analysis. These devices were integrated into a custom-built enclosure equipped with a monitor for system visualization. The setup was connected to a primary computer for comprehensive data logging. A specialized software application, Cool Term, facilitated efficient data capture and storage in CSV format. This integrated system enabled precise control of experimental parameters, real-time system behavior monitoring, and comprehensive data acquisition for subsequent analysis. The schematic of the test rig is shown in Figure 2, and the photo of some of the components of the test rig is shown in Figure 3 and Figure 4.

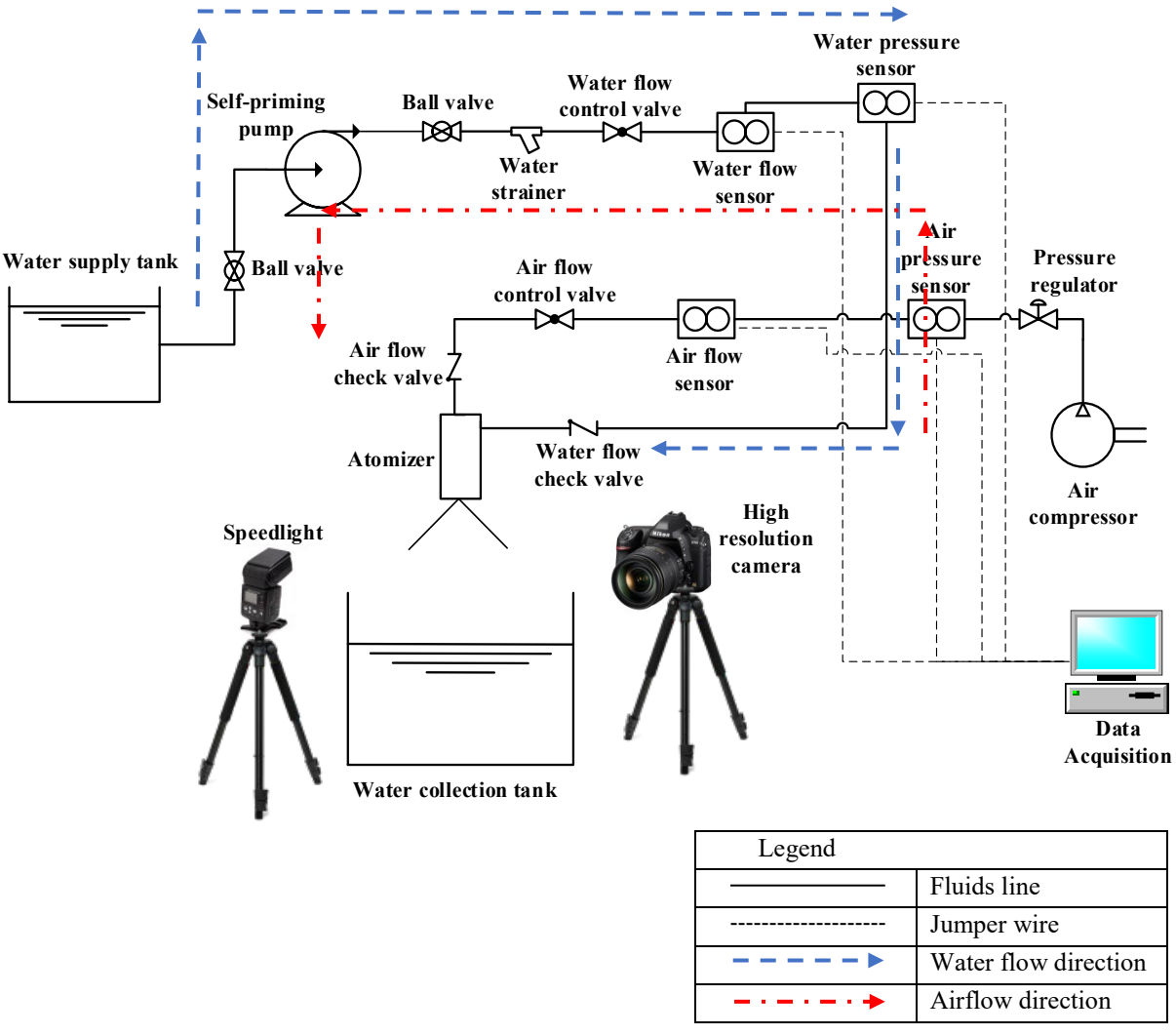

Figure 2. Schematic of the test rig

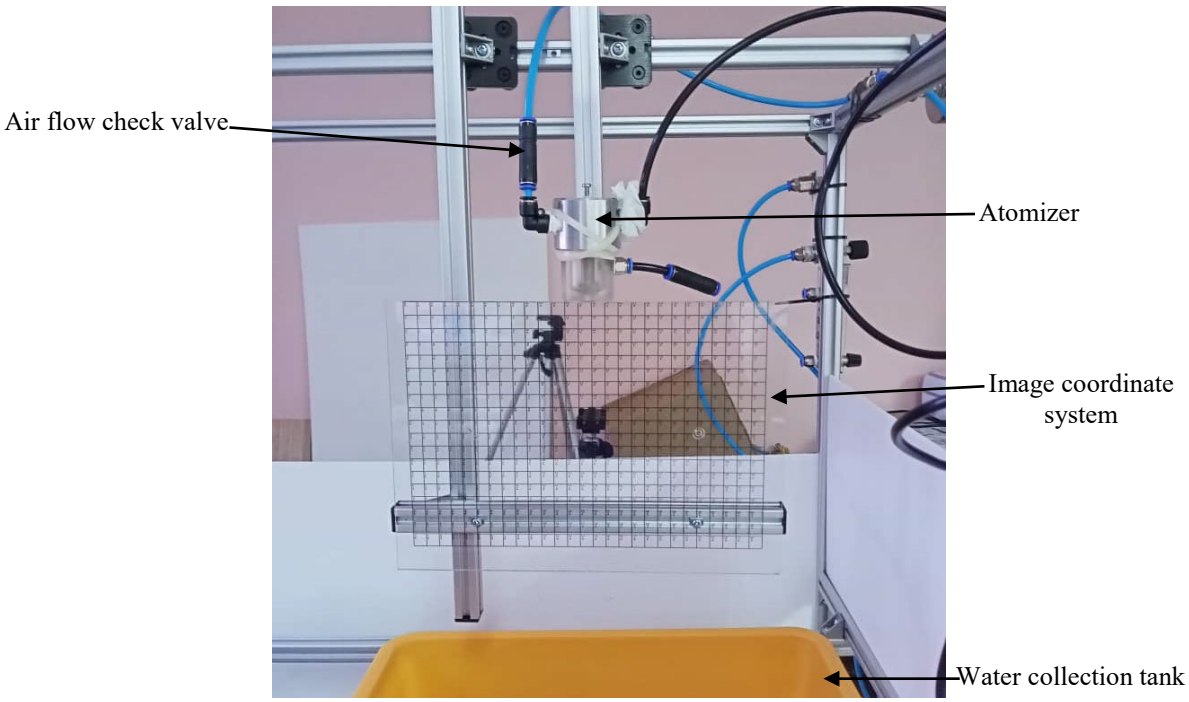

Figure 3. Photo of some components of the test rig

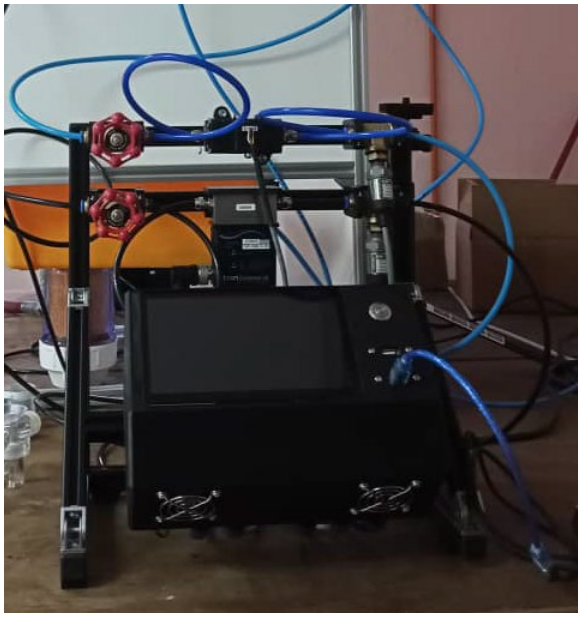

Figure 4. The data acquisition system comprises Arduino and Raspberry Pi

2.3 Design of Experiment

Experimental planning was executed using a Box-Behnken Design (BBD) methodology, aligned with the recommendations of Anderson and Whitcomb [31]. Given the multifactorial nature of the study, with multiple levels and quantitative factors, response surface methodology was deemed appropriate. Among available response surface designs, BBD was selected for its efficiency in minimizing experimental runs and avoiding extreme operating conditions. The experimental matrix was generated and analyzed using Minitab software. Three critical factors, identified through dimensional analysis and considerations of liquid disintegration regimes, were incorporated into the experiment: liquid Reynolds number, gas Reynolds number, and swirl chamber length-to-orifice diameter ratio. The specific levels of these variables and their corresponding notations are detailed in Table 2. The range and levels of the liquid Reynolds number are chosen based on the internal flow regimes of a pipe. A laminar flow is observed with the liquid Reynolds number below 2300. Starting from liquid Reynolds number 2300 to 4000, the flow regimes experience a transition regime. A liquid Reynolds number of more than 4000 causes the internal flow to transform to turbulent flow regimes. The position of the swirl-generating vane is the basis of the range and levels of the swirl chamber length-to-discharge orifice diameter ratio. The lowest level represents the nearest position of the swirl-generating vane to the discharge orifice. This can be

considered a position with the shortest possible length of the swirl chamber. The middle level is the position at the conic section, and the highest is at the pressure sensor port. The change in swirl chamber length may affect the stability of a swirl atomizer's internal flow, as Kim et al. [32] reported. Variations in swirl chamber lengths may also represent the swirling strength of the atomizing liquid. Fong et al. [33] showed that swirling modifies droplet transport in the spray cross-section, enhances break-up, and reduces the D_{32} globally.

Table 2. Factors and their levels

Factor	Notation	Factor Level		
		-1	0	+1
Liquid Reynolds number	*L*	847	1270	2540
Gas Reynolds number	*G*	0	728	1514
Swirl chamber length to discharge	*S*	1.5	4.5	9.0

The arrangement of three factors with 3 levels in BBD can be shown graphically using a cube, as shown in Figure 5. BBD avoided the extreme conditions of the experiment, which was illustrated by the absence of a black dot at every edge of the cube. The experiment was performed following the BBD arrangement with 15 experimental runs. This is based on the interlocking as in Figure 5(b), which illustrates 12 experimental points and repetition of the central point up to 3 times. The matrix of the 15 experimental runs is shown in Table 3.

Table 3. Experimental order matrix

Run Order	*L*	*G*	*S*
1	847	1514.0	4.5
2	1270	728.0	4.5
3	1270	0.4	1.5
4	1270	1514.0	9.0
5	2540	728.0	9.0
6	2540	1514.0	4.5
7	1270	0.4	9.0
8	2540	0.4	4.5
9	1270	728.0	4.5
10	847	728.0	9.0
11	847	728.0	1.5
12	1270	1514.0	1.5
13	2540	728.0	1.5
14	847	0.4	4.5
15	1270	728.0	4.5

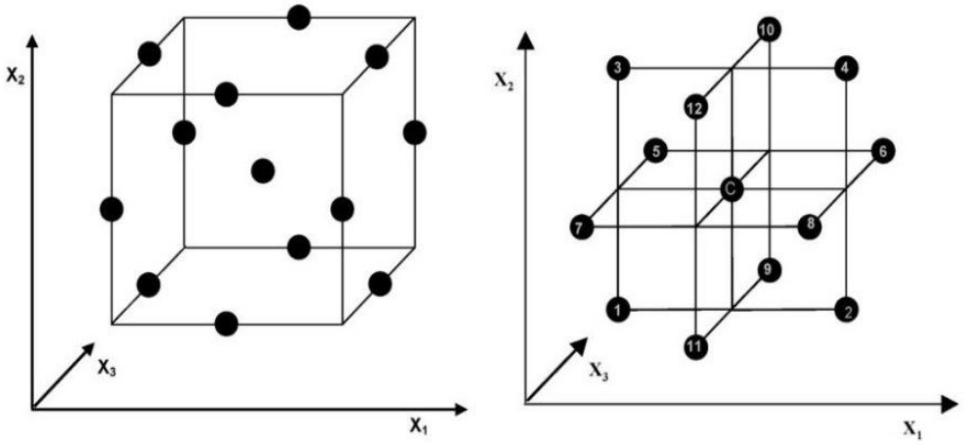

(a) (b)

Figure 5. Graphical layout of BBD for three variables with: (a) BBD cube and (b) three interlocking and central point

2.4 Data Extraction and Analysis

2.4.1 Image acquisition

Shadowgraphy, an optical imaging technique, was utilized to capture visual records of the spray and internal flow patterns. This method involves recording the backlit shadows of droplets [34]. The imaging system consisted of a digital single-lens reflex (DSLR) camera equipped with a speedlight and a diffuser to ensure even illumination. To prevent the camera from being exposed to the spray, a lens extender was attached to the camera, allowing for magnified images without compromising equipment. Images were captured at an aperture of f/18 and ISO 100 to optimize image quality. A remote control triggered the camera, minimizing vibrations and ensuring image clarity. A shadowgraph image of a grid of 1cm squares named droplet coordinate system was superimposed on the images to establish a spatial reference system, enabling accurate measurements and analysis. Image processing software, specifically ImageJ, was employed to extract quantitative data from the captured images. The shadowgraph image of the droplet coordinate system is illustrated in Figure 6.

Figure 6. Shadowgraph image of the droplet coordinate system

2.4.2 Droplet diameter data extraction

Droplet diameter measurements were obtained by analyzing stacked spray images within a defined coordinate system. The stacking process enabled the identification of the initial droplet formation point. The images are then cropped a few mm higher than the initial droplet before undergoing droplet diameter measurement. Images cropping into the region of interest are essential to ensure that only the final droplets are included in the measurement of the droplet diameter and avoid the secondary droplets (not the main droplets) known as satellite droplets.

The extraction of a droplet diameter is based on the steps suggested by Asgarian et al. [35] and other proposed steps. The steps start with background subtraction, in which the spray images are subtracted from a previously captured background image (an image without spray) to isolate the spray images from the background. Then, the images underwent threshold adjustment, which involved determining lower and upper-intensity values for pixels either automatically or interactively to analyze each droplet. This technique highlights the borders of in-focus droplets while filtering out those that are out of focus. The image must be in black and white binary format before filling the area within the boundary of each droplet with the Fill Holes command. Next, the Fill Holes command was executed. This step is where droplet areas are filled using the fill holes command after binarization, which closes any enclosed boundary regardless of its shape. This process may leave some noise in the form of crescents. These droplet images then proceed to remove noise using the Remove Outliers function. This replaces a pixel with the median value of surrounding pixels if it deviates from the median by more than a specified threshold. This filter operates on black-and-white images, independent of the binarisation threshold. Another parameter for this filter is the size of the circular area, measured in pixels, used to calculate the median. The Analyze Particles command was applied to obtain the droplet diameter. The value of circularity was set from 0.686 to 1.00. The value 0.686 was selected to avoid the extreme droplet elongation, which rarely occurs in a completely atomized liquid. Generally, circularity, C in the image processing field is defined as in Eq. (9):

$$\mathrm{C} = \frac{4A\pi}{P^2} \tag{8}$$

where A and P are the area and perimeter of the droplet, respectively.

2.4.3 Data analysis

In the current work, mathematical models were developed to predict the spray characteristics of the swirl effervescent atomization and to conduct a statistical analysis of the interaction of the parameters on the response surface using Minitab 20.0 statistical software. The droplet mean diameter will be modeled based on response surface methodology using the Box-Behnken experimental design technique. The development of mathematical models begins with response surface

regression analysis for all terms (linear, square, and interactions) via analysis of variance (ANOVA). ANOVA determined the significant terms and factors indicated by the p-value < 0.05. The objective of ANOVA is to identify the RSM model that best fits all the data from which the data are tested [36]. Then, the insignificant terms and factors were eliminated. Insignificant terms and factors will result in a high percentage of errors in the model and need to be removed. Next, the model with reduced terms and factors was re-analyzed using response surface regression to determine a new model. Finally, the new model was verified by constructing a few residual plots to compare how well the known data is within the fitted line. A random plot (no significant trend) of the experimental points indicates a well-fitted model.

The estimated regression coefficient for uncoded units is obtained and shown in Eq. (10):

$$D_{32} = 3986 - 0.711\mathrm{L} + 0.488\mathrm{G} - 146.8\mathrm{S} - 0.00063 \quad (9)$$

where L is the notation for liquid Reynolds number, G is the notation for gas Reynolds number, and S is the notation for swirl chamber length to diameter ratio.

The trend analysis of the acquired data was also performed alongside the development of the prediction model. The effect of the individual factor (liquid Reynolds number, gas Reynolds number, and swirl chamber length to orifice diameter ratio) on the droplet mean diameter was also presented.

3. RESULTS AND DISCUSSION

The resultant droplet means the diameter of the Sauter mean diameter of the new swirl effervescent atomizer is presented. The results discussed the effect of the individual factors (i.e., liquid Reynolds number, gas Reynolds number, and swirl chamber length to discharge orifice diameter ratio) and the empirical model generated by the Minitab software.

3.1 Effect of Individual Factors

The Sauter mean diameter is one example of a representative mean diameter to characterize the distribution of droplets emanating from an atomizer. The investigation of the relation of the liquid Reynolds number on the D_{32} is presented in Figure 7. The range of the liquid Reynolds number starts with 847, representing a laminar flow regime inside the discharge orifice. The mid value of the liquid Reynolds number 1270 is also an indicator representing the flow regime inside the discharge orifice as laminar flow. The highest setting of the liquid Reynolds number is 2540, which suggests that the internal flow is in a transition regime.

The increase of the liquid Reynolds number from 847 to 2540 causes the D_{32} to decrease. However, the decrement of D_{32} is insignificant, with the number of liquid Reynolds increasing from 847 to 1270. This may be attributed to the flow regime for both liquid Reynolds numbers and laminar flow regimes. The nature of steady flow in the laminar does not significantly affect the D_{32}. A different phenomenon was observed with liquid Reynolds number 2540 as the flow is in a transition regime. The initiation of unsteady flow induces more instability, which causes the bulk liquid to break into finer droplets. In addition, the effect of liquid Reynolds number on D_{32}, which causes the decrement of D_{32}, was also reported by Saha et al. [37] for swirl atomization.

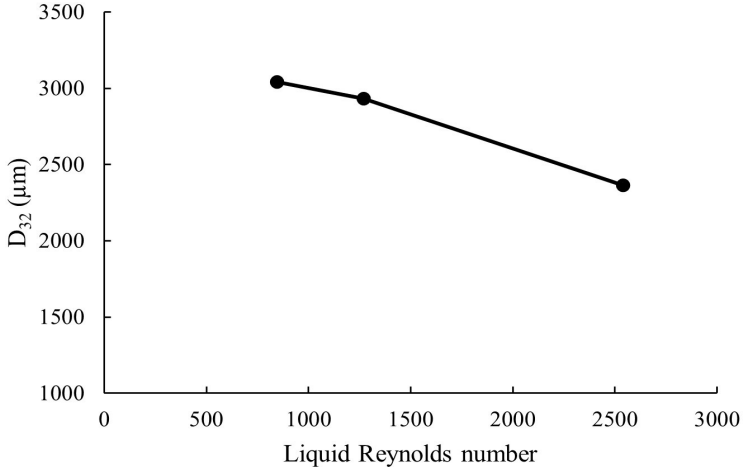

Figure 7. Effect of liquid Reynolds number on D_{32}

The effect of the gas Reynolds number on the D_{32} is presented in Figure 8. The investigated gas Reynolds number ranges from 0 to 1514, equivalent to the GLR range from 0 to 0.032. The line graph illustrates an inversely proportional trend of D_{32} with the gas Reynolds number. The trend is similar to that observed in the previous line graph, as shown in Figure 5. Both the gas and liquid Reynolds numbers cause a decrease in the droplet to mean diameter. However, a steeper reduction of D_{32} was observed with the change of gas Reynolds number. The D_{32} drops from 3041.518 μm to 2362.312 μm with the increase of liquid Reynolds number, but gas Reynolds number causes a drop of D_{32} from 3182.254 μm to 2140.818 μm.

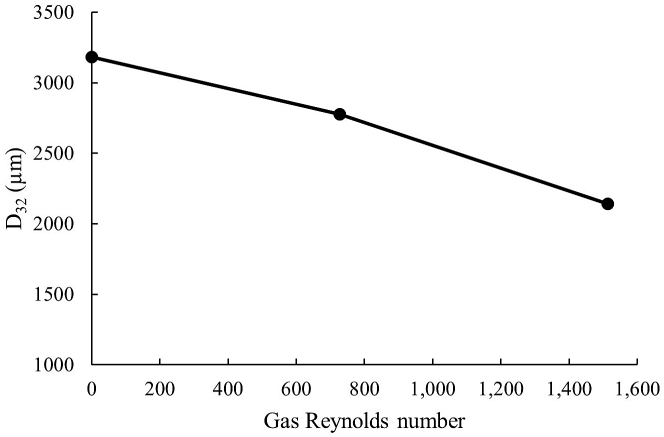

Figure 8. Effect of gas Reynolds number on D_{32}

Figure 9 illustrates the relationship between the swirl chamber length to discharge orifice diameter ratio (L/do), and the Sauter mean diameter (D_{32}). The analysis investigated L/do ratios of 1.5, 4.5, and 9.0, where higher ratios correspond to decreased swirling strength. The results demonstrate that increasing the L/do ratio progressively increases D32 from 2,615.493 μm to 2,971.457 μm. This trend can be attributed to the reduction in swirling strength associated with larger L/do ratios. Rashad et al. [38] reported similar findings, noting that extending the swirl chamber length beyond its optimal value intensifies energy losses due to enhanced liquid-wall interactions, subsequently diminishing the liquid's angular momentum. Notably, the observed variation in D_{32} across the tested L/do range is less pronounced than the variations induced by liquid and gas Reynolds numbers, indicating that the L/do ratio exerts a relatively minor influence on droplet size distribution.

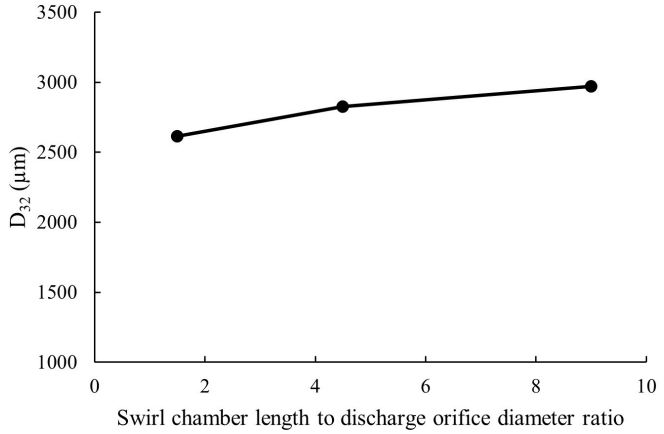

Figure 9. Effect of swirl chamber length to discharge orifice diameter ratio on D_{32}

3.2 Empirical Model

A response surface regression analysis examined the relationship between the Sauter mean diameter and three factors: liquid Reynolds number, gas Reynolds number, and the ratio of swirl chamber length to discharge orifice diameter. The analysis utilized data in coded units, followed by an Analysis of Variance (ANOVA), as presented in Table 4. The ANOVA results indicate that linear and interaction terms significantly contribute to the model ($p < 0.05$ for linear terms, $p = 0.001$; interaction terms, $p = 0.076$), while quadratic terms were statistically insignificant. Consequently, the model was refined by excluding the quadratic terms, with the updated ANOVA results presented in Table 5. The regression coefficients for uncoded units were derived and expressed in Equation (10). To validate the model's adequacy, residual analysis was performed. The residual versus fitted values plot (Figure 10) reveals no discernible patterns, confirming the model's compliance with regression assumptions and ANOVA requirements. Additional validation was conducted using a residual versus observation order plot to assess potential temporal effects in the data. Independent residuals show no trends or patterns when displayed in time order. Patterns in the points indicate that residuals near each other may be correlated and, thus, not independent. The plot in Figure 11 has an ideal plot with the residuals falling randomly around the center line and no visible trends observed. The relationship between the actual and predicted Sauter mean diameter is shown in Figure 12. The observation on the graph visualizes that the generated prediction model for the Sauter mean diameter has predicted the Sauter mean diameter with minimum error. This can be shown by the closeness of the points to the regression line $y = x$. Another tool to quantify the error is called relative standard error (RSE), which is defined by Goodarzi et al. [39] as in Eq. (11). In general, estimates are considered statistically reliable if the RSE of the estimate is less than 30% [40] and RSE for the Sauter mean diameter is 9.0%.

$$\text{RSE} = \sqrt{\frac{\sum(Actual\ Response - Predicted\ Response)^2}{\sum(Actual\ Response)^2}} \tag{11}$$

Table 4. ANOVA for Sauter mean diameter model

Source	DF	Adj SS	Adj MS	F-value	P-value
Model	9	6008415	667602	4.40	0.059
Linear	3	4487374	1495791	9.86	0.015
L	1	699770	699770	4.61	0.084
G	1	3104140	3104140	20.46	0.006
S	1	638471	638471	4.21	0.950
Square	3	255974	85325	0.56	0.663
*L***L*	1	24255	24255	0.16	0.706
*G***G*	1	212199	212199	1.40	0.290
*S***S*	1	44922	44922	0.30	0.610
2-Way Interaction	3	1942979	647660	4.27	0.076
*L***G*	1	750818	750818	4.95	0.077
*L***S*	1	1102420	1102420	7.27	0.043
*G***S*	1	101403	101403	0.67	0.451

Table 5. ANOVA for Sauter mean diameter model (reduced terms)

Source	DF	Adj SS	Adj MS	F-value	P-value
Model	9	5752441	958740	7.56	0.006
Linear	3	4663499	1554500	12.26	0.002
L	1	842750	842750	6.65	0.033
G	1	3142227	3142227	24.78	0.001
S	1	624412	624412	4.92	0.057
2-Way Interaction	3	1984418	661473	5.22	0.028
*L***G*	1	748154	748154	5.90	0.041
*L***S*	1	1146567	1146567	9.04	0.017
*G***S*	1	100999	100999	0.80	0.398

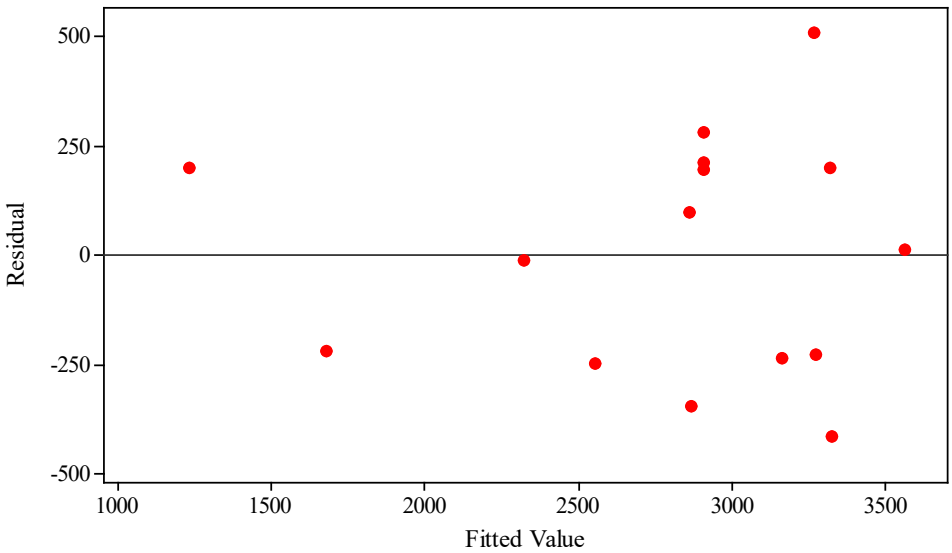

Figure 10. Residuals versus fits for Sauter mean diameter model (reduced terms)

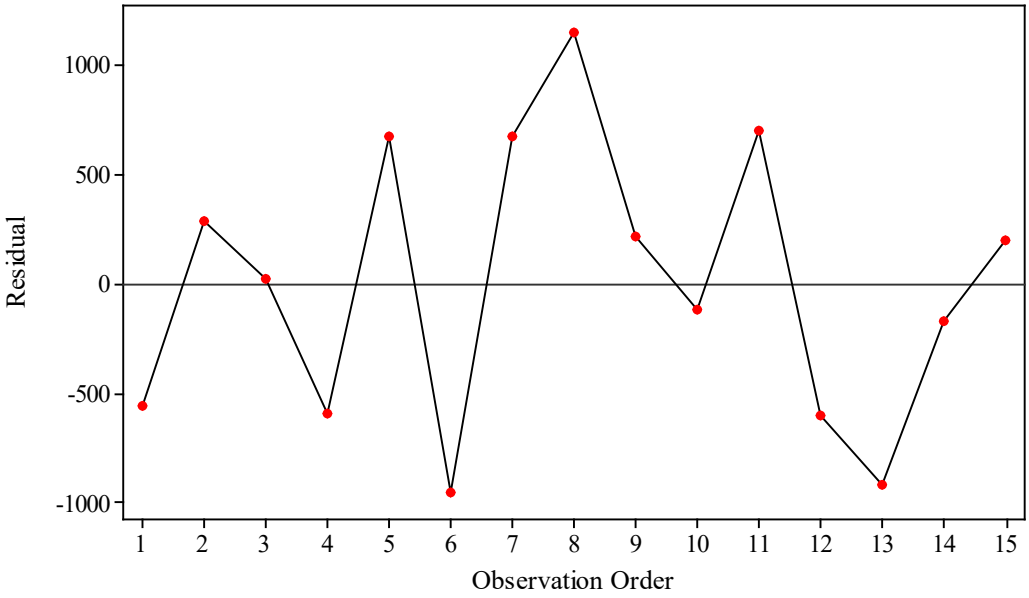

Figure 11. Residuals versus observation order plot for Sauter mean diameter model (reduced terms)

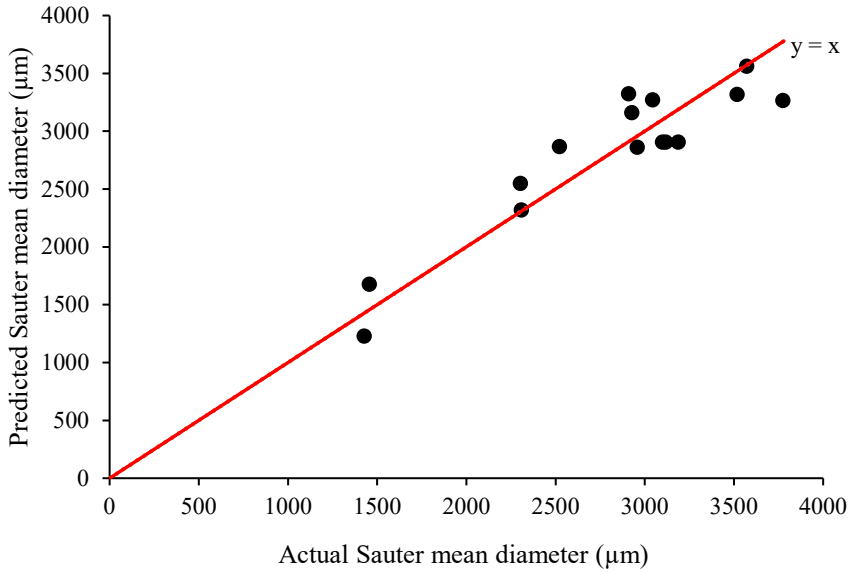

Figure 12. Actual versus predicted Sauter mean diameter

4. CONCLUSIONS

Swirl effervescent atomization is a hybrid mechanism combining swirl and effervescent atomization. The characteristics study of the discharging Sauter means diameter was conducted. The Box-Behnken design was employed to reduce the number of experiments and predict an empirical model. A novel swirl effervescent was fabricated. Shadowgraph and image processing were used to measure the individual droplet diameter. The acquired droplet diameters were analyzed and presented as droplet mean diameters. Sauter mean diameter, D_{32} was chosen in this study, considering this mean diameter is applied for mass transfer, and the equation includes the surface area. Surface area is among the vital characteristics of liquid atomization since one of the purposes of atomization is to increase the surface area of a bulk liquid. It was found that both the gas and liquid Reynolds numbers cause a decrease in the Sauter mean diameter. However, a steeper reduction of the Sauter mean diameter was observed with the change of gas Reynolds number. The swirl chamber length to discharge orifice diameter ratio does not significantly affect the Sauter mean diameter. The mathematical model was developed using Minitab and tested for goodness-of-fit using various tools. It was observed that the developed mathematical model could accurately predict the correlation of the Sauter mean diameter with the liquid Reynolds number, gas Reynolds number, and swirl chamber length to discharge orifice diameter ratio. The results of this study may offer good assistance in understanding the mechanics of swirl effervescent atomization.

ACKNOWLEDGEMENTS

The Ministry of Higher Education Malaysia supported this research through Geran Penyelidikan Fundamental (FRGS), FRGS/1/2019/TK03/ UITM/02/14 and Dana Dalaman Fakulti (DANA DDF), 600-TNCPI 5/3/DDF (KPK) (001/2023). This acknowledgement is also extended to UiTM's Research Management Center (RMC).

CONFLICT OF INTEREST

The authors declare no conflicts of interest.

AUTHORS CONTRIBUTION

Z. A. Ghaffar (Conceptualization; Methodology; Formal analysis; Data curation; Investigation; Writing - original draft)

S. Kasolang (Conceptualization; Methodology; Validation; Writing - review & editing; Funding acquisition; Supervision)

Ahmad H. A. Hamid (Conceptualization; Methodology; Validation; Writing - review & editing; Funding acquisition; Supervision)

M. H. Mamat (Writing - review & editing; Funding acquisition)

AVAILABILITY OF DATA AND MATERIALS

The data supporting this study's findings are available on request from the corresponding author.

ETHICS AND STATEMENT

Not applicable

REFERENCES

[1] A. Kushari, S. Pandey, "A controllable twin-fluid internally mixed swirl atomizer," *Recent Patents on Mechanical Engineering*, vol. 1, no. 1, pp. 45–50, 2008.

[2] A. H. Lefebvre, V. G. McDonell, Atomization and Sprays, 2nd Eds. Boca Raton: CRC Press, 2017.

[3] G. Li, C. Li, "Experimental study on the spray steadiness of an internal-mixing twin-fluid atomizer," *Energy*, vol. 226, p. 120394, 2021.

[4] Z. A. Ghaffar, A. H. A. Hamid, M. S. F. M. Rashid, "Spray characteristics of swirl effervescent injector in rocket application: A review," *Applied Mechanics and Materials*, vol. 225, pp. 423-428, 2012.

[5] M. Mlkvik, P. Stähle, H. P. Schuchmann, V. Gaukel, J. Jedelsky, M. Jicha, "Twin-fluid atomization of viscous liquids: The effect of atomizer construction on breakup process, spray stability and droplet size," *International Journal of Multiphase Flow*, vol. 77, pp. 19–31, 2015.

[6] S. Wachter, T. Jakobs, T. Kolb, "Experimental investigation on the influence of system pressure on resulting spray quality and jet breakup applying pressure adapted twin-fluid nozzles," *International Journal of Multiphase Flow*, vol. 125, p. 103189, 2020.

[7] H. Liu. Science and Engineering of Droplets: Fundamentals and Applications. 1st Ed. New York: Noyes Publications, 2000.

[8] M. Lörcher, F. Schmidt, D. Mewes, "Effervescent atomization of liquids," *Atomization and Sprays*, vol. 15, no. 2, pp. 145–168, 2005.

[9] R. A. Mugele, H. D. Evans, "Droplet size distribution in sprays," *Industrial and Engineering Chemistry*, vol. 43, no. 6, pp. 1317–1324, 1951.

[10] J. Van Strien, S. Vahaji, P. Lappas, D. Morton, K. Inthavong, "Spatial and temporal characterization of droplet diameter and velocities of a nasal spray atomization," *Aerosol Science and Technology*, vol. 58, no. 6, pp. 610–629, 2024.

[11] J. Barroso, A. Lozano, F. Barreras, E. Lincheta, "Analysis and prediction of the spray produced by an internal mixing chamber twin-fluid nozzle," *Fuel Processing Technology*, vol. 128, pp. 1–9, 2014.

[12] S. K. Vankeswaram, R. Sakthikumar, S. Deivandren, J. D. C. Hu, "Evaluation of spray characteristics of aviation biofuels and Jet A-1 from a hybrid airblast atomizer," *Experimental Thermal and Fluid Science,* vol. 142, p. 110820, 2023.

[13] R. H. Myers, D. C. Montgomery, C. M. Anderson-Cook. Response surface methodology: Process and product optimization using designed experiments, 3rd Eds. New Jersey: John Wiley and Sons, 2009.

[14] H. Liu, K. Wang, W. Schlindwein, M. Li, "Using the Box-Behnken experimental design to optimise operating parameters in pulsed spray fluidised bed granulation," *International Journal of Pharmaceutics*, vol. 448, no. 2, pp. 329–338, 2013.

[15] S. L. C. Ferreira, R. E. Bruns, H. S. Ferreira, G. D. Matos, J. M. David, G. C. Brandão, et al., "Box-Behnken design: An alternative for the optimization of analytical methods," *Analytica Chimica Acta*, vol. 597, no. 2, pp. 179–186, 2007.

[16] P. G. Mathews. Design of experiments with MINITAB. 1st Ed. Milwaukee: ASQ Quality Press, 2005.

[17] A. Dean, D. Voss, D. Draguljić, Design and Analysis of Experiments, 2nd Eds. Cham: Springer International Publishing AG, 2017.

[18] O. Porwal, "Box-Behnken design-based formulation optimization and characterization of spray-dried rutin loaded nanosuspension: State of the art," *South African Journal of Botany*, vol. 149, pp. 807–815, 2022.

[19] R. Yakut, "Response surface methodology-based multi-nozzle optimization for electrospray cooling," *Applied Thermal Engineering*, vol. 236, p. 121914, 2024.

[20] J. Qiu, Q. Zhang, B. Jiang, M. Tang, L. Zhou, "Analysis of the effect of water film dust removal of a tunnel's full-section fog screen dust capture system," *Chemical Engineering Research and Design*, vol. 209, pp. 258–271, 2024.

[21] P. Saiteja, B. Ashok, "Study on interactive effects of CRDi engine operating parameters through RSM based multi-objective optimization technique for biofuel application," *Energy*, vol. 255, p. 124499, 2022.

[22] Z. A. Ghaffar, S. Kasolang, A. H. A. Hamid, C. S. Ow, N. R. Nik Roselina, "Design, development and performance evaluation of new swirl effervescent injector," *Jurnal Teknologi*, vol. 75, no. 1, pp. 19-25, 2015.

[23] Z. A. Ghaffar, S. Kasolang, A. H. A. Hamid, "Optimization of swirl effervescent spray dispersity via response surface methodology," *International Transaction Journal of Engineering, Management, & Applied Sciences & Technology*, vol. 13, no. 13, p. 13A13H, 2022.

[24] J. D. Whitlow, A. H. Lefebvre, R. J. Rollbuhler, "Experimental studies on effervescent atomizers with wide spray angles," in *AGARD Conference Proceedings: Fuels and Combustion Technology for Advanced Aircraft Engines*, pp. 1-11, 1993.

[25] J. Jedelsky, M. Jicha, "Novel modifications of twin-fluid atomizers: performance, advantages and drawbacks," in *Proceedings of the 23rd Annual Conference on Liquid Atomization and Spray Systems ILASS-Europe,* vol. 23, pp. 1-5, 2010.

[26] M. Ochowiak, "Discharge coefficient of effervescent atomizers with the swirl motion phenomenon," *Experimental Thermal and Fluid Science,* vol. 79, pp. 44–51, 2016.

[27] L. Liu, N. Pei, R. Zhao, L. Tian, R. Duan, Y. Zhang, et al., "Effect of the two-phase hybrid mode of effervescent atomizer on the atomization characteristics," *Open Physics*, vol. 17, no. 1, pp. 960–965, 2019.

[28] J. Xie, L. Liu, X. Huo, X. Liu, R. Duan, "Numerical and experimental study of wire mesh in the swirl effervescent atomization," *Physics of Fluids*, vol. 35, no. 8, 2023.

[29] Z. A. Ghaffar, S. Kasolang, A H. A. Hamid, Z. Eshak, "Experimental analysis of tangential-vane swirl atomizer spray angle," *Journal of Advanced Research in Fluid Mechanics and Thermal Sciences*, vol. 101, no. 2, pp. 1–7, 2023.

[30] B. Stewart. Adventures in Arduino. 1st Ed. West Sussex: John Wiley and Sons, 2015.

[31] M. J. Anderson, P. J. Whitcomb. DOE Simplified: Practical Tools for Effective Experimentation, 3rd Eds. Boca Raton: CRC Press, 2007.

[32] S. Kim, T. Khil, D. Kim, Y. Yoon, "Effect of geometric parameters on the liquid film thickness and air core formation in a swirl injector," *Measurement. Science and Technology*, vol. 20, no. 1, p. 015403, 2009.

[33] K. O. Fong, X. Xue, R. Osuna-Orozco, A. Aliseda, "Gas-liquid coaxial atomization with swirl in high-pressure environments," *International Journal of Multiphase Flow*, vol. 174, p. 104767, 2024.

[34] V. S. Jagadale, D. Deshmukh, D. Hanstorp, Y. N. Mishra, "Bubble dynamics and atomization of acoustically levitated diesel and biodiesel droplets using femtosecond laser pulses," *Scientific Reports*, vol. 14, no. 1, p. 8285, 2024.

[35] A. Asgarian, Z. Yang, Z. Tang, M. Bussmann, K. Chattopadhyay, "An image feature consolidation technique (IFCT) to capture multi-range droplet size distributions in atomizing liquid sheets," *Experiments in Fluids*, vol. 61, no. 14, pp. 1-22, 2020.

[36] U. M. R. Paturi, N. S. Reddy, S. Cheruku, S. K. R. Narala, K. K. Cho, M. M. Reddy, "Estimation of coating thickness in electrostatic spray deposition by machine learning and response surface methodology," *Surface and Coatings Technology*, vol. 422, p. 127559, 2021.

[37] A. Saha, J. D. Lee, S. Basu, R. Kumar, "Breakup and coalescence characteristics of a hollow cone swirling spray," *Physics of Fluids*, vol. 24, no. 12, pp. 1-21, 2012.

[38] M. Rashad, H. Yong, Z. Zekun, "Effect of geometric parameters on spray characteristics of pressure swirl atomizers," *International Journal of Hydrogen Energy*, vol. 41, no. 35, pp. 15790–15799, 2016.

[39] M. Goodarzi, P. Shahbazikhah, M. R. Sohrabi, M. Fathabadi, S. H. Nouri, "Direct orthogonal signal correction-partial least squares for simultaneous spectrophotometric determination of sulfamethoxazole and trimethoprim in pharmaceutical formulation and synthetic samples," *Journal of the Chilean Chemical Society*, vol. 54, no. 3, pp. 309–313, 2009.

[40] R. J. Klein, S. E. Proctor, M. A. Boudreault, K. M. Turczyn, "Healthy People 2010 criteria for data suppression," *Healthy People 2010 Statistical Notes*, vol. 24, no. 1237, pp. 1–12, 2002.